Effects of Trimethylaluminum Vapor Pressure and Exposure Time on Inorganic Loading in Vapor Phase Infiltrated PIM-1 Polymer Membranes

Benjamin C. Jean,[†] Yi Ren,[‡] Emily K. McGuinness,[†] Ryan Lively,[‡] and Mark D. Losego[†] *

[†]School of Materials Science and Engineering, [‡]School of Chemical and Biomolecular Engineering, Georgia Institute of Technology, Atlanta, GA 30332, United States

Corresponding Author: losego@gatech.edu

Abstract

Vapor phase infiltration (VPI) is a post-polymerization modification method for infusing inorganic clusters into a polymer to create organic-inorganic hybrid materials with properties that are unique from the parent polymer. The properties of these hybrid materials can vary with the amount of VPI generated inorganic loading. However, the relationship between VPI processing conditions and inorganic loading is still not fully understood. In this paper, the effects of VPI dose pressure and exposure time on inorganic loading are explored using the technologically relevant membrane material known as "polymer of intrinsic microporosity 1" (PIM-1). At sufficiently low dose pressures and infiltration times (i.e., before saturation), inorganic loading can be controlled with both vapor pressure and exposure time. However, inorganic loading appears to saturate for this system when the polymer's functional groups become fully populated with bound VPI precursors. These experimental results can be understood with the use of a recently developed reaction-diffusion model for VPI. Critical to applying this model to these post-deposition measurements is re-normalizing the mass loading to the total number of functional groups in the polymer

Introduction

Vapor phase infiltration (VPI) is an emerging processing technology that infiltrates vapor phase metal-organic precursors into bulk polymers to create novel organic-inorganic hybrid materials.[1] Because it is a vapor-phase technique, VPI can be used to modify organic materials without affecting early fabrication steps used to synthesize the polymer and/or its final form factor (fiber, fabric, membrane, etc.). VPI has been shown to alter a number of material properties, including solvent stability, mechanical strength, and electrical conductivity.[2-4] VPI-created hybrid materials have been used to improve the performance of numerous systems including solar cells[5], membranes[2, 6] and UV resistant coatings.[7]

Recently, VPI has been used to improve the stability and chemical separation performance of polymer membranes. Membrane-based separations are significantly more energy efficient and have lower capital costs than traditional thermal separation methods.[8] However, polymer membranes are often unstable, and thus unusable, for non-aqueous chemical mixtures including organic solvents. They tend to swell, plasticize and even dissolve in organic solvents. Prior work has demonstrated that VPI-created AlO_x-PIM-1 hybrid membranes are chemically stable in a variety of organic solvents and exhibit excellent separation performance.[2] Because of its small pores size and large free volume, PIM-1 is of great interest as a membrane for chemical separations.[9] This makes PIM-1 an ideal candidate for VPI membrane modification.

VPI process conditions, like process temperature, are known to significantly alter the physicochemical structure of the final materials, including the quantity of infiltrated inorganic and its chemical bonding to the polymer.[10] The amount of infiltrated inorganic has been shown to affect the mechanical strength, chemical stability, and thermal degradation of the final infiltrated material.[3, 11] Despite the known effects of inorganic loading on hybrid properties, the relationships between VPI processing parameters and final hybrid structure are still not well understood. Many material property changes in VPI treated materials occur due to chemical cross-linking as well as the concentration of inorganic entrapment within the polymeric material.[12, 13] Given that both of these physicochemical features are dependent on VPI processing conditions, clarifying the role that processing parameters play on inorganic loading will be extremely important to further optimize desired material properties via VPI.

This paper aims to explain how VPI processing conditions affect inorganic loading. More specifically, this paper elucidates the relationship that processing pressure and exposure time have on inorganic loading using the test case of trimethylaluminum (TMA) VPI into polymer of intrinsic microporosity 1 (PIM-1). A recently developed reaction-diffusion model for VPI is then used to explain the experimental observations.[14] Trends in inorganic loading can be better understood by renormalizing the mass uptake curves as a function of total mass uptake, rather than normalized mass.

Experimental Methods

PIM-1 Synthesis: PIM-1 was synthesized using the low polycondensation method developed by Budd *et al.*[15] 5,5′,6,6′-tetrahydroxy-3,3,3′,3′-tetramethyl-1,1′-spirobisindane (TTSBI) is purchased from Alfa Aesar with a purity of 97% and tetrafluoroterephthalonitrile (TFTPN) is purchased from Sung-Young Chemical Limited with a purity of 99%. TTSBI is purified via a hot recrystallization method where TTSBI is first dissolved in hot MeOH and recrystallized from dichloromethane. TFTPN is purified under vacuum sublimation. Purified TTSBI and TFTPN were carefully weighed at a molar ratio of 1:1 and dissolved in DMF using a round bottom flask placed in oil bath for temperature control. When oil bath temperature reached 65 ºC, potassium carbonate fine powders were added to the solution at a ratio of 2.5:1:1 with respect to the monomers. The reaction ran under inert atmosphere, either via a nitrogen flow or stagnant nitrogen balloon for 72 hours. After reaction was complete, PIM-1 was dissolved in chloroform and precipitated from MeOH for purification. Further purification of PIM-1 was achieved by soaking PIM-1 in DMF for 24 hours, and then re-soaking in MeOH for 72 hours before collecting by filtration. In this work, the PIM-1 fibers were gained by mixing a total of 4 PIM-1 synthesis run, with molecular weights of 116k, 225k, 135k and 143k respectively, each with a mass of 12-13g. The PDI (polydispersity index) was around 4 for all 4 synthesis runs.

Vapor Phase Infiltration: Vapor phase infiltration was conducted in a custom-built 1 ft^3 cubic, hot-walled reactor. A full description of the VPI set up can be found here.[2] PIM-1 was soaked in methanol and then dried in a fume hood to reset the polymer structure prior to infiltration.[16] PIM-1 was then placed within the reactor which was kept at 90 °C and purged with ultrahigh purity (UHP, Airgas, 99.999%) nitrogen for 5 hours to remove excess water and methanol. The chamber was then pumped down to rough vacuum (~30 mTorr) and isolated. The metal-containing precursor, trimethylaluminum (TMA, 98%, Strem Chemicals, DANGER: pyrophoric) was then dosed from a room temperature precursor bottle into the chamber to an intentional partial pressure of between 0.1 Torr and 0.6 Torr. For our 28 L chamber that uses valves with a flow coefficient

of Cv = 0.27, this corresponds to opening the valve to the TMA precursor for between 0.5s s and 3s. This environment was then held for between 0.5 hours and 40 hours before being pumped down to 30 mTorr for 5 min and then purged with nitrogen for 25 hours to remove any excess TMA. Then fibers were exposed to a water vapor dose and exposure of 1.8 Torr for 5 hours before a final nitrogen purge. Co-reacting with water vapor creates an air stable hybrid material infiltrated with $MO_x(OH)_y$ inorganics within the polymer free volume. Experiments with TMA were conducted at dose pressures of 0.1 Torr, 0.2 Torr, 0.3 Torr, and 0.6 Torr to study the effect of precursor dose pressure on mass uptake. The pressure was recorded using a Baratron capacitance manometer.

Reaction Diffusion Model: The reaction diffusion model is a recently developed and published phenomenological model used to describe transport in VPI processes that accounts for both diffusion and reaction kinetics and assumes a second order reaction rate.[14] The reaction diffusion model also introduces a hindering factor, K', to account for the reduction in diffusivity due to the extent of precursor reaction with the polymer. This model attempts to account for non-Fickian behavior in the VPI process and has been previously shown to do a reasonable job of capturing the experimentally observed phenomena. A MATLAB code to run this model is readily available on GitHub.[18]

Thermogravimetric Analysis: Thermogravimetric (TGA, PerkinElmer TGA 4000) analysis was performed in air to determine the inorganic loading in VPI treated PIM-1 fibers. PIM-1 fibers were heated at 10 °C /min from 30 ºC to 120 °C. This temperature was held for 50 minutes to remove any adsorbed water. After this step, the fibers were heated at 10 °C /min to 700 °C, at which all organic components were combusted. Compressed air was constantly flowed through the TGA (Airgas). Inorganic mass loading was determined to be the difference between the final mass and the mass after the 120 °C drying step.

Raman Spectroscopy: Raman spectroscopy was used to determine changes in vibrational states of PIM-1 fibers before and after inorganic loading with VPI. The intensity of specific organic vibrational modes were found to decay with increasing inorganic loading. PIM-1 fibers were analyzed on a Renishaw Raman Spectrometer - vis / near-IR using a 785 nm laser.

Results and Discussion

Effects of precursor dose pressure on VPI in PIM-1

We previously demonstrated post-polymerization VPI modification of PIM-1 with TMA-H_2O to form PIM-1/AlO_x hybrid membranes that are chemically stable against dissolution and swelling in various organic solvents and exhibited nearly identical separation performance irrespective of solvent.[2] Here, we re-examine this system to understand how altering vapor pressure and exposure time affects the amount of inorganic loading in the PIM-1 fibers, and how our ex situ observations of final inorganic mass loading can be interpreted in context with our recently reported reaction-diffusion model for VPI process kinetics.[14] Exact fitting to a quantitative model fit is difficult to determine from solely from *ex situ* data due to diffusivity and reaction rate uncertainty. However, these findings can be examined to inform VPI process trends.

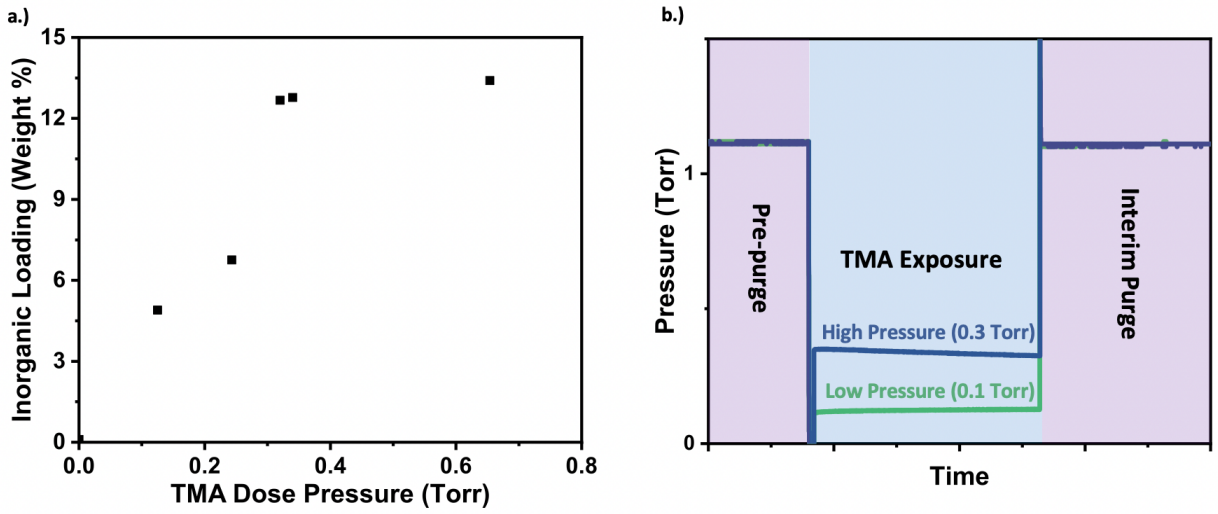

Fig. 1. (a) Plot showing bound inorganic loading weight percent as measured by TGA in air as a function of TMA dose pressure for PIM-1/AlOx hybrid membrane fibers after five hour TMA exposures; (b) Pressure curves for the VPI TMA exposure step for PIM-1/AlOx at 0.1 and 0.3 Torr.

Fig. 1(a) plots the inorganic loading in PIM-1 hybrid films after VPI at 90 °C as a function of the TMA process pressure used for infiltration. At this process temperature, inorganic loading in PIM-1 increases with TMA partial pressure up to about 0.3 Torr TMA, at which point inorganic loading plateaus. This result suggests some form of saturation or equilibrium is reached above process pressures of 0.3 Torr TMA at this temperature. Note that in these experiments, membranes are exposed to TMA for 5 hours and then the chamber is purged with flowing nitrogen for 25 hours in an attempt to fully remove any TMA precursor that is unbound to the polymer membrane. Thus, the inorganic loadings reported in Fig. 1(a) are believed to be the result of TMA precursor molecules that chemically adduct to the polymer. The electron lone pair on the nitrile group (-C≡N) of PIM-1 is a Lewis base that likely forms a dative bond (Lewis adduct) with the Lewis acid metal-organic precursor TMA. Similar adducts have also been reported between TMA and nitro and amine functional groups.[13] We interpret the plateau of inorganic mass-loading in Fig. 1(a) as indication of all nitrile groups in the PIM-1 membrane being adducted to TMA molecules during the TMA exposure step. The theoretical saturated inorganic loading for the case of each TMA molecule adducted to a nitrile site would be 18.3 weight %. The apparent saturation point of 13.4 weight % inorganic corresponds to approximately 0.69 TMA molecules per functional group.

Kinetic Considerations of VPI in PIM-1

Interpreting process mechanisms from post-processing analysis like that reported in Fig. 1(a) is frought with complications. For example, several explanations can be posited. One possible explanation is that the process is reactant limited at low TMA partial pressures. In other words, below 0.3 Torr, there are less TMA molecules than PIM-1 functional groups and all of the TMA precursor in the chamber is consumed via reaction with the polymer's functional groups. However, this explanation is unlikely, given that no significant decrease in chamber partial pressure is observed during the TMA exposure step as shown in Fig. 1(b). For clarity, Fig. 1(b) illustratively shows the pressure above and below saturation; while only two pressure curves are

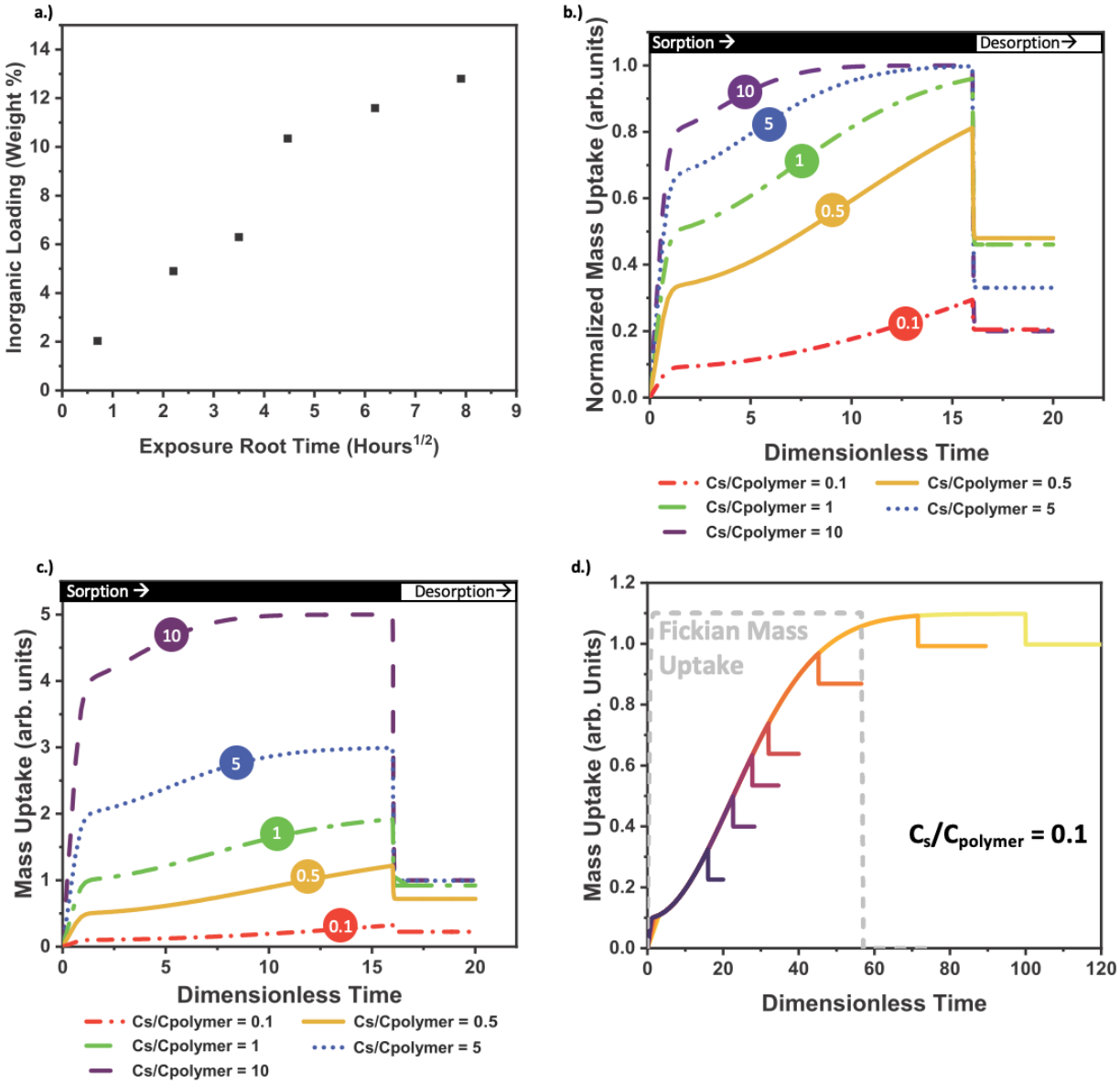

Fig. 2. (a) Experimental inorganic loading in PIM-1 infiltrated at 0.1 Torr as a function of precursor exposure time; (b) Plot of reaction-diffusion modeled mass uptake as a function of dimensionless time , $\sqrt{\frac{D_0 t}{l^2}}$, for several $C_s/C_{polymer}$ values; (c) Mass uptake as a function of $C_s/C_{polymer}$ value; (d) Reaction-diffusion modeled mass uptake as a function of dimensionless time for $C_s/C_{polymer}$ = 0.1 (red curve in Fig. 2(c)). For reference, a purely fickian mass uptake is plotted in grey.

shown, all pressure curves follow the same trend. The second possible explanation is that the process is saturating at varying loading concentrations dependent upon the precursor's partial pressure (activity), similar to a Langmuir isotherm.[17] However, Langmuir isotherms represent thermodynamic equilibrium conditions, and in this case the overpressure was purposefully removed for an extended time (25 hrs) in an attempt to eliminate the established equilibrium between vapor and physically dissolved TMA species. Thus, this explanation is also likely not true. For both of these explanations, extending the TMA exposure time should not increase the

amount of inorganic at these low dose pressures (<0.3 Torr). Thus, to adequately discredit these two interpretations, a second set of experiments are conducted to track the mass loading as a function of TMA exposure time at the lowest TMA partial pressure (0.1 Torr).

Fig. 2(a) plots the inorganic mass loading in PIM-1 as a function of TMA exposure time (in root time) for VPI at 90 °C and 0.1 Torr TMA. Immediately evident is that more inorganic can be infiltrated into PIM-1 if the TMA exposure step is extended beyond the 5 h (ca. 2.2 $h^{0.5}$) tested in Fig. 1. Thus, the lower loadings observed at 0.1 Torr and 0.2 Torr in Fig. 1(a) must be a consequence of incomplete transport, not a thermodynamically-limited saturation point nor a full consumption of precursor. In fact, for "long enough" exposure times (>8 $h^{0.5}$ or >65 h), mass loadings nearly equivalent to the apparent saturation point in Fig. 1(a) are possible (ca. 13 wt% inorganic).

Here, we posit that these observations can be explained by our recently reported VPI reaction-diffusion model.[14] This model includes the dimensionless parameter $\frac{C_s}{C^o_{polymer}}$ where C_s is the equilibrium surface concentration of physically sorbed VPI precursors and $C^o_{polymer}$ is the density of the polymer's functional groups that react with or adduct to the VPI precursor. In this model, the C_s values should be directly proportional to the precursor vapor pressure during VPI, so increasing precursor partial pressure should increase $\frac{C_s}{C^o_{polymer}}$ for a given polymer chemistry. In the prior report, Ren *et al.* plotted mass uptake (M_t) for the VPI reaction-diffusion model normalized to the total theoretical saturation inorganic mass uptake (M_∞).[14] However, normalizing to total theoretical saturation mass uptake can lead to challenges in interpreting *ex situ* measurements like those made here where the total theoretical saturation mass uptake during the process is unknown. This potential confusion is highlighted with Fig. 2(b) which plots calculations of the mass uptake data as a function of the dimensionless time interval, $\sqrt{\frac{D_0 t}{l^2}}$, for various $\frac{C_s}{C^o_{polymer}}$ ratios using mass uptake (M_t) normalized to the total possible maximum mass uptake, also known as the theoretical saturation mass uptake (M_∞). Here, the total possible mass uptake includes not only the chemically adducted immobilized inorganic species determined by $C^0_{polymer}$, but also the physically dissolved precursor species in equilibrium with the precursor overpressure determined by C_s; these "physically dissolved" species have the potential to desorb out of the polymer during the pumping and purging processes prior to process completion. As a result, these physically dissolved species are not measured in an *ex situ* analysis. The loss of these dissolved but unbound species is made more likely if a long "purge" step is included between the precursor exposure step and the co-reactant (water) exposure step, as was done here (25 h nitrogen purge). This "purge" step permits sufficient time for nearly all these unbound dissolved species to desorb from the polymer. When normalized in this way (Fig. (2(b)), the remaining bound precursors after the desorption step appear to be somewhat "random" with increasing $\frac{C_s}{C^o_{polymer}}$ ratio, increasing with ratios of 10, 0.1, 5, 1, 0.5. However, this is really a consequence of a combination of incomplete saturation and varying physically dissolved unbound precursor sorption.

Here, we argue that a better way to translate the reaction-diffusion model for the analysis of *ex situ* VPI mass loading data is to compare it to the output of the reaction-diffusion model when it is renormalized to the total possible mass of bound inorganic species—essentially the concentration of polymer functional groups that react with the precursor, $C^o_{polymer}$. Practically, renormalizing this model is rather simple and can be done by multiplying through by M_∞ to plot

M_t, which is already normalized to the number of functional groups in the polymer. Fig. 2(c) plots the renormalized mass uptake as a function of the dimensionless time interval, $\sqrt{\frac{D_0 t}{l^2}}$.–Here, $C_s/C_{polymer}$ is again varied to simulate an increase in precursor pressure. With this normalization scheme, the systematic increases in physically dissolved but chemically unbound species during sorption as well as chemically bound species after desorption (i.e., what is detected with *ex situ* analysis) with increasing precursor partial pressure is readily apparent (i.e., the mass uptakes increase monotonically for increasing $C_s/C_{polymer}$ ratios of 0.1, 0.5, 1, 5, 10). Furthermore, at lower $C_s/C_{polymer}$ ratios (e.g., $C_s/C_{polymer} < 2$ for the Damkohler number and reaction constant illustratively chosen here), full saturation of the bound precursors has likely not been reached within the dimensionless time interval of exposure chosen here (16 times the characteristic diffusion length).

Finally, Fig. 2(d) re-calculates the condition for $C_s/C_{polymer} = 0.1$ (the red curve in Fig. 2(c) that is shown to be far from saturation) but for increasing amounts of dimensionless time, up to 100 times the characteristic diffusion length. At each of these dimensionless times, we also allow desorption to occur. We see that around a dimensionless time of 70, saturation is now finally reached, with the bound species after desorption having a M_t value of 1, just like the higher $C_s/C_{polymer}$ ratios achieved in shorter time periods in Fig. 2(c). Thus, from Fig. 2(c) and Fig. 2(d) the saturation value for the fully bound inorganic precursors species is the same at low and high VPI precursor pressures but the rate to reach saturation increases with increasing VPI precursor pressures. This result makes intuitive sense given that the saturation concentration should depend upon the total concentration of polymer functional groups reactive towards the precursor, and thus only dependent on the polymer chemistry. The increase in VPI process kinetics with increasing $C_s/C_{polymer}$ ratio is interesting given that this provides an additional strategy for controlling VPI process kinetics beyond chemistry and temperature.

To summarize, for a fixed vapor-polymer system such as TMA with PIM-1 under same temperature, the saturation value should be the same and is merely dependent on the density of polymer functional groups that is reactive to precursor vapor. Changing the pressure will change the rate of infiltration, and thus the time required to reach saturation, and changing the exposure time will change the level of saturation. For this system, it appears that given enough time for any pressure, the saturation loading can be reached and will remain the same. For example, when infiltrating at a pressure of 0.1 Torr, it takes about 35 hours to reach the saturation value.

Here, the *ex situ* experimental measurements of mass uptake with precursor exposure time presented in Fig. 2(a) can be explained by the slow kinetics towards saturation of bound precursors at low precursor partial pressures illustrated in the reaction-diffusion model results of Fig. 2(d). While an exact quantitative model fit is difficult to determine from *ex situ* data alone because of uncertainties in the diffusivities and reaction constants, these general trends in process rates to be compelling for further validating the reaction-diffusion transport model in explaining the vapor phase infiltration process. In general, from this analysis, we recommend that to conduct ex situ mass analysis on VPI loaded polymer, experiments should include long purge steps that effectively remove any dissolved but unbound precursors prior to analysis and then multiple precursor exposure times should be examined until a saturation point is determined—like was done in Fig. 2(a). These methods are in fact similar to saturation curves run for atomic layer deposition processes.[19]

Raman Analysis

Finally, we comment briefly about another method for ex situ mass uptake analysis in VPI modified polymers—Raman spectroscopy. Fig. 3 plots Raman spectra collected from PIM-1 membranes prior to and after 90 °C VPI modification at varying TMA partial pressures (Fig. 3(a) and 3(b)) and varying exposure times (Fig. 3(c)). Here, the nitrile stretch, methyl stretch, and CH_2 wagging modes of PIM-1 are highlighted at 2240 cm^{-1}, 1400 cm^{-1}, and1316 cm^{-1} respectively. [20,21] Note all spectra have been normalized to the CH_2 wagging mode at 1316 cm^{-1} of pure PIM-1 because DFT calculations predict no significant interactions between inorganic and these PIM-1 moieties.[22] In contrast, these Raman spectra clearly show a reduction in the nitrile and methyl stretches upon infiltration. As depicted in Fig. 3(d), the nitrile and methyl groups extend farther from the PIM-1 backbone than the hydrogens of the methylene groups in the cyclopentane ring, making them more susceptible to restricted motions. Here, we interpret the observed reduction in nitrile and methyl intensities as indicative of the infiltrated inorganic AlO_xH_y clusters constraining the vibrations of these side groups. As a result, the reduction in nitrile and methyl Raman vibrational stretch intensities appear to be indicative of inorganic loading quantity within these hybrid membranes. As an example, Fig. 3(b) and Fig. 3(c) plot the normalized spectral intensities of the nitrile stretch as a function of the precursor partial pressure and precursor exposure time respectively, for conditions explored above that are known by TGA to alter the inorganic mass loading. These figures confirm monotonic decrease in nitrile stretch intensity with increasing inorganic loading. To determine the approximate functional form for this apparent correlation between Raman intensity and inorganic loading fraction, Fig. 3(e) plots the inorganic loading determined by TGA versus the nitrile stretch intensity normalized to the CH_2 wagging mode

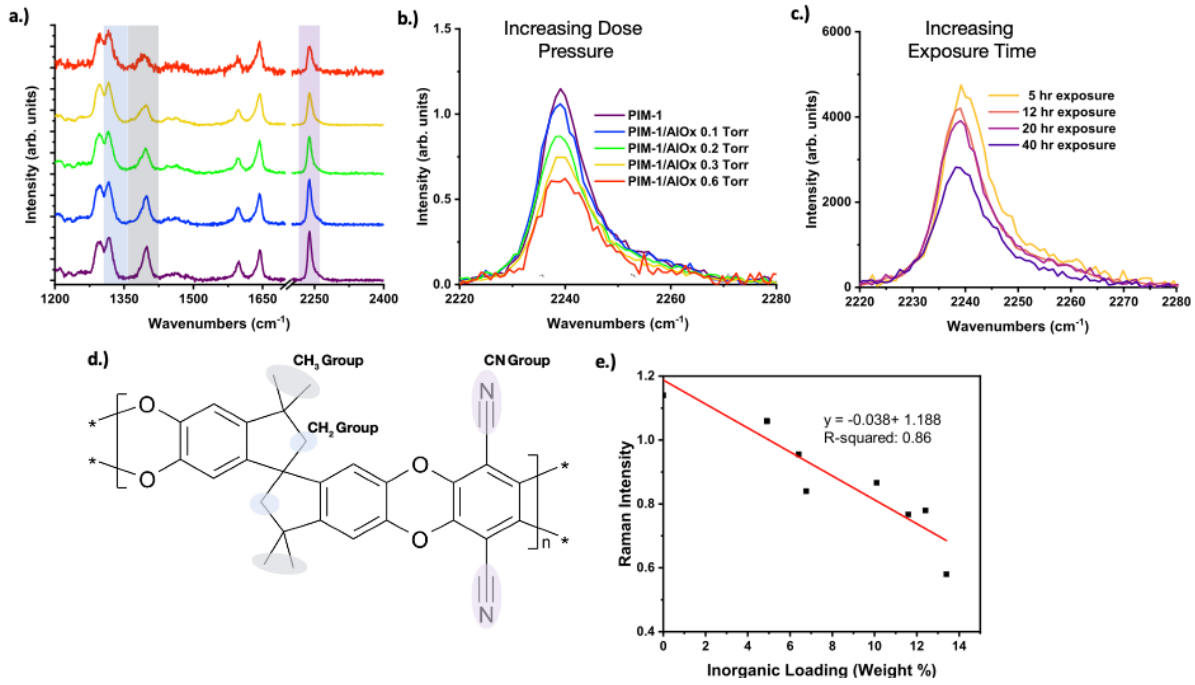

Fig. 3. (a) Raman spectra of PIM-1 infiltrated at various precursor pressures (b) Nitrile stretch of PIM-1 infiltrated at various precursor pressures; (c) Nitrile stretch of PIM-1 infiltrated with various exposure times; (d) PIM-1 polymer indicating functional groups; (e) Normalized intensity of the Nitrile stretch as a function of inorganic loading

intensity for both the precursor partial pressure and exposure time data series presented in Fig. 3(b) and 3(c). Linear regression provides the following predictive equation: $y = -0.038x + 1.188$ with an R-squared value of 0.86, where weight percent represents the x value and nitrile stretch intensity represents the y value. This plot suggests a somewhat linear correlation between Raman intensity and inorganic loading fraction.

Conclusions

This work analyzes the relationship between VPI processing conditions and inorganic loading. The effects of the processing parameters of dose pressure and exposure time play a significant role in the final VPI treated material structure and morphology, which can lead to variations in material properties. In this paper, the effect of processing pressure was explored as a method to vary inorganic loadings, which is the zeroth order determinant of properties. We demonstrated that the process pressure dependencies observed via *ex situ* mass loading analysis could be explained with the recently developed reaction-diffusion model for VPI if the model's mass is renormalized to the concentration of reactive functional groups within the infiltrated polymer. Interestingly, we show that the total saturation mass loading after full desorption is a constant with VPI process pressure, but the VPI process kinetics can vary significantly with VPI process pressure. These insights provide new understanding to how to control mass loading in VPI processes.

References

(1) Ingram, W. F.; Jur, J. S. Properties and Applications of Vapor Infiltration into Polymeric Substrates. *JOM* **2019**, *71* (1), 238-245. DOI: 10.1007/s11837-018-3157-9.

(2) McGuinness, E. K.; Zhang, F.; Ma, Y.; Lively, R. P.; Losego, M. D. Vapor Phase Infiltration of Metal Oxides into Nanoporous Polymers for Organic Solvent Separation Membranes. *Chemistry of Materials* **2019**, *31* (15), 5509-5518. DOI: 10.1021/acs.chemmater.9b01141.

(3) Gregorczyk, K. E.; Pickup, D. F.; Sanz, M. G.; Irakulis, I. A.; Rogero, C.; Knez, M. Tuning the Tensile Strength of Cellulose through Vapor-Phase Metalation. *Chemistry of Materials* **2015**, *27* (1), 181-188. DOI: 10.1021/cm503724c.

(4) Wang, W.; Yang, F.; Chen, C.; Zhang, L.; Qin, Y.; Knez, M. Tuning the Conductivity of Polyaniline through Doping by Means of Single Precursor Vapor Phase Infiltration. *Advanced Materials Interfaces* **2017**, *4* (4), 1600806. DOI: https://doi.org/10.1002/admi.201600806.

(5) Obuchovsky, S.; Deckman, I.; Moshonov, M.; Segal Peretz, T.; Ankonina, G.; Savenije, T. J.; Frey, G. L. Atomic layer deposition of zinc oxide onto and into P3HT for hybrid photovoltaics. *Journal of Materials Chemistry C* **2014**, *2* (42), 8903-8910, 10.1039/C4TC01629G. DOI: 10.1039/C4TC01629G.

(6) Chen, X.; Wu, L.; Yang, H.; Qin, Y.; Ma, X.; Li, N. Tailoring the Microporosity of Polymers of Intrinsic Microporosity for Advanced Gas Separation by Atomic Layer Deposition. *Angewandte Chemie International Edition* **2021**, *60* (33), 17875-17880. DOI: https://doi.org/10.1002/anie.202016901.

(7) Azpitarte, I.; Botta, G. A.; Tollan, C.; Knez, M. SCIP: a new simultaneous vapor phase coating and infiltration process for tougher and UV-resistant polymer fibers. *RSC Advances* **2020**, *10* (27), 15976-15982, 10.1039/D0RA02073G. DOI: 10.1039/D0RA02073G.

(8) Sholl, D. S.; Lively, R. P. Seven chemical separations to change the world. *Nature* **2016**, *532* (7600), 435-437. DOI: 10.1038/532435a.

(9) Budd, P. M.; McKeown, N. B.; Ghanem, B. S.; Msayib, K. J.; Fritsch, D.; Starannikova, L.; Belov, N.; Sanfirova, O.; Yampolskii, Y.; Shantarovich, V. Gas permeation parameters and other physicochemical properties of a polymer of intrinsic microporosity: Polybenzodioxane PIM-1. *Journal of Membrane Science* **2008**, *325* (2), 851-860. DOI: https://doi.org/10.1016/j.memsci.2008.09.010.

(10) Gong, B.; Peng, Q.; Jur, J. S.; Devine, C. K.; Lee, K.; Parsons, G. N. Sequential Vapor Infiltration of Metal Oxides into Sacrificial Polyester Fibers: Shape Replication and Controlled Porosity of Microporous/Mesoporous Oxide Monoliths. *Chemistry of Materials* **2011**, *23* (15), 3476-3485. DOI: 10.1021/cm200694w.

Pilz, J.; Coclite, A. M.; Losego, M. D. Vapor phase infiltration of zinc oxide into thin films of cis-polyisoprene rubber. *Materials Advances* **2020**, *1* (6), 1695-1704, 10.1039/D0MA00304B. DOI: 10.1039/D0MA00304B.

Dandley, E. C.; Needham, C. D.; Williams, P. S.; Brozena, A. H.; Oldham, C. J.; Parsons, G. N. Temperature-dependent reaction between trimethylaluminum and poly(methyl methacrylate) during sequential vapor infiltration: experimental and ab initio analysis. *Journal of Materials Chemistry C* **2014**, *2* (44), 9416-9424, 10.1039/C4TC01293C. DOI: 10.1039/C4TC01293C.

(11) Azpitarte, I.; Zuzuarregui, A.; Ablat, H.; Ruiz-Rubio, L.; López-Ortega, A.; Elliott, S. D.; Knez, M. Suppressing the Thermal and Ultraviolet Sensitivity of Kevlar by Infiltration and Hybridization

with ZnO. *Chemistry of Materials* **2017**, *29* (23), 10068-10074. DOI: 10.1021/acs.chemmater.7b03747.
(12) Bamford, J. T.; Smith, R. A.; Leng, C. Z.; Gutekunst, W. R.; Losego, M. D. Measuring the Glass Transition Temperature of Vapor-Phase-Infiltrated AlOx-PS-r-PHEMA Organic–Inorganic Hybrid Thin-Film Materials. *Macromolecules* **2021**. DOI: 10.1021/acs.macromol.1c00691.
Chan, K.; Gleason, K. K. Initiated Chemical Vapor Deposition of Linear and Cross-linked Poly(2-hydroxyethyl methacrylate) for Use as Thin-Film Hydrogels. *Langmuir* **2005**, *21* (19), 8930-8939. DOI: 10.1021/la051004q.
(13) Yang, F.; Brede, J.; Ablat, H.; Abadia, M.; Zhang, L.; Rogero, C.; Elliott, S. D.; Knez, M. Reversible and Irreversible Reactions of Trimethylaluminum with Common Organic Functional Groups as a Model for Molecular Layer Deposition and Vapor Phase Infiltration. *Advanced Materials Interfaces* **2017**, *4* (18), 1700237. DOI: https://doi.org/10.1002/admi.201700237.
(14) Ren, Y.; McGuinness, E. K.; Huang, C.; Joseph, V. R.; Lively, R. P.; Losego, M. D. Reaction–Diffusion Transport Model to Predict Precursor Uptake and Spatial Distribution in Vapor-Phase Infiltration Processes. *Chemistry of Materials* **2021**, *33* (13), 5210-5222. DOI: 10.1021/acs.chemmater.1c01283.
(15) Kim, J.-U.; Cha, S.-H.; Shin, K.; Jho, J. Y.; Lee, J.-C. Preparation of Gold Nanowires and Nanosheets in Bulk Block Copolymer Phases under Mild Conditions. *Advanced Materials* **2004**, *16* (5), 459-464. DOI: https://doi.org/10.1002/adma.200305613.
(16) Jue, M. L.; McKay, C. S.; McCool, B. A.; Finn, M. G.; Lively, R. P. Effect of Nonsolvent Treatments on the Microstructure of PIM-1. *Macromolecules* **2015**, *48* (16), 5780-5790. DOI: 10.1021/acs.macromol.5b01507.
(17) Kecili, R.; Hussain, C. M. Chapter 4 - Mechanism of Adsorption on Nanomaterials. In *Nanomaterials in Chromatography*, Hussain, C. M. Ed.; Elsevier, 2018; pp 89-115.
(18) *accesible at:* https://github.com/yren48/Reaction_Diffusion_Model
(19) Mackus, A. J. M.; Garcia-Alonso, D.; Knoops, H. C. M.; Bol, A. A.; Kessels, W. M. M. Room-Temperature Atomic Layer Deposition of Platinum. *Chemistry of Materials* **2013**, *25* (9), 1769-1774. DOI: 10.1021/cm400274n.
(20) Číhal, P.; Dendisová, M.; Švecová, M.; Hrdlička, Z.; Durďáková, T.-M.; Budd, P. M.; Harrison, W.; Friess, K.; Vopička, O. Sorption, swelling and plasticization of PIM-1 in methanol-dimethyl carbonate vapour mixtures. *Polymer* **2021**, *218*, 123509. DOI: https://doi.org/10.1016/j.polymer.2021.123509.
(21) Lin-Vien, D.; Colthup, N. B.; Fateley, W. G.; Grasselli, J. G. CHAPTER 2 - Alkanes. In *The Handbook of Infrared and Raman Characteristic Frequencies of Organic Molecules*, Lin-Vien, D., Colthup, N. B., Fateley, W. G., Grasselli, J. G. Eds.; Academic Press, 1991; pp 9-28.
(22) Liu, Y. M., Emily; Jean, Benjamin ; Li, Yi; Ren, Yi; Gonzalez del Rio, Beatriz; Lively, Ryan; Losego, Mark; Ramprasad, Rampi. Vapor Phase Infiltration of Polymer of Intrinsic Microporosity 1 (PIM-1) with Trimethylaluminum (TMA) and Water: A combined computational and experimental study. *J. Phys. Chem* **2022**.